Bioactive Materials 42 (2024) 194–206

Contents lists available at ScienceDirect

Bioactive Materials

journal homepage: www.keaipublishing.com/en/journals/bioactive-materials

Dynamic compliance penis enlargement patch

Rui Zheng [a,b,1], Wenwen Zhong [c,1], Muyuan Chai [a,d,**], Xuetao Shi [a,b,e,*]

[a] National Engineering Research Centre for Tissue Restoration and Reconstruction, South China University of Technology, Guangzhou, 510006, PR China
[b] School of Materials Science and Engineering, South China University of Technology, Guangzhou, 510640, PR China
[c] Department of Urology, The Sixth Affiliated Hospital, Sun Yat-sen University, Guangzhou, 510655, PR China
[d] Dongguan Key Laboratory of Smart Biomaterials and Regenerative Medicine, The Tenth Affiliated Hospital, Southern Medical University, Dongguan, 523000, PR China
[e] Key Laboratory of Biomedical Engineering of Guangdong Province, South China University of Technology, Guangzhou, 510006, PR China

ARTICLE INFO

Keywords:
Polyvinyl alcohol
Hydrogel
Negative Poisson's ratio
Crystallization enhancement
Penis enlargement

ABSTRACT

Men are particularly sensitive to penis size, especially those with a deformed or injured penis. This can lead to a strong desire for penis enlargement surgery. Given the ethical sensitivities of the penis, penile implants need to be developed with both efficacy and safety. In this study, a polyvinyl alcohol (PVA) patch for penile enlargement prepared via cyclic freeze–thaw cycles and alkaline treatment. The PVA hydrogels treated with 5 M NaOH had the best mechanical properties and stability. A negative Poisson's ratio structure is incorporated into the design of the enlargement patch, which allows it to conform well to the deformation of the penis. In rabbit models, the enlarged patches can effectively enlarge the penis without degradation or fibrosis while maintaining long-term stability *in vivo*. This innovation not only provides a safe option for patients in need of penile enlargement but also promises to make a broader contribution to the field of dynamic tissue repair.

1. Introduction

Throughout history, penis size has been a concern for men[1–4]. Individuals who are overly preoccupied with perceived defects or deficiencies in the appearance of the penis may have a form of penile dysmorphic disorder, which can be considered a form of body dysmorphic disorder according to the Diagnostic and Statistical Manual of Mental Disorders, Fifth Edition (DSM-5) [2]. Recently, due to psychological causes, such as locker room syndrome and congenital small penis syndrome [5], and acquired trauma or tumor treatment resulting in penile defects [6,7], the demand for penis enlargement has increased. However, clinically safe and effective penile enlargement methods to meet this high demand is lacking. Conservative treatments such as filler injections or negative pressure devices can temporarily increase penis size, but their long-term effectiveness is limited [1,8,9]. Surgical implantation of penis enlargement patches is an option for permanent enlargement, but surgery is risky and can result in numerous complications. To achieve long-term, stable penis enlargement with the least possible side effects, the penis enlargement patch needs to be specifically designed for the unique microenvironment of the penis.

The penis has a highly dynamic microenvironment [10,11] with macroscopic deformations caused by flaccidity to erection expanding or contracting simultaneously in multiple directions; these deformations are characterized by typical negative Poisson's ratio (NPR) strains. Conventional penile patches can cause stress concentrations during erection, which can lead to problems such as patch displacement, painful erections, and penile curvature [6,12]. By employing a structural design that dynamically adapts and responds, an NPR penile patch can effectively avoid these problems [13]. The design of NPR materials is relatively challenging. As a result, increased focus has been on creating structures that exhibit NPR properties. For example, Chansoria and colleagues designed several types of NPR patches to mimic the motion of dynamic human organs [14], facilitating the for the development of future biomimetic patches. Jiang et al. used 3D printing techniques to fabricate an NPR thermoplastic polyurethane elastomer scaffold for intervertebral disc replacement [15]. The modified scaffold

Peer review under responsibility of KeAi Communications Co., Ltd.
* Corresponding author. National Engineering Research Centre for Tissue Restoration and Reconstruction, South China University of Technology, Guangzhou, 510006, PR China.
** Corresponding author. National Engineering Research Centre for Tissue Restoration and Reconstruction, South China University of Technology, Guangzhou, 510006, PR China.
E-mail addresses: chaimuyuan@126.com (M. Chai), shxt@scut.edu.cn (X. Shi).
[1] Both authors contributed equally.

https://doi.org/10.1016/j.bioactmat.2024.08.039
Received 31 May 2024; Received in revised form 28 August 2024; Accepted 29 August 2024

demonstrated exceptional energy absorption and dissipation characteristics. However, due to limitations in the raw materials and preparation methods, NPR structural scaffolds have not been used in the field of penile enlargement.

With the growth of the field of biomaterials, an increasing number of implant materials, including silicone (such as Penuma®) [16,17], hyaluronic acid [18], and polylactic acid [19,20], have been approved by the U.S. Food and Drug Administration, and many physicians have attempted to use these materials for penile augmentation. However, all of these materials have significant drawbacks. For example, compared with the human penis, silicone implants have greater stiffness, which can lead to complications such as hematoma and hypertrophic scarring [16,21]. Hyaluronic acid [6] has poor mechanical properties and is easily degraded; thus, it has difficulty maintaining the penile shape over time. The degradation products of polylactic acid can cause inflammation, resulting in significant side effects. Another category of potential

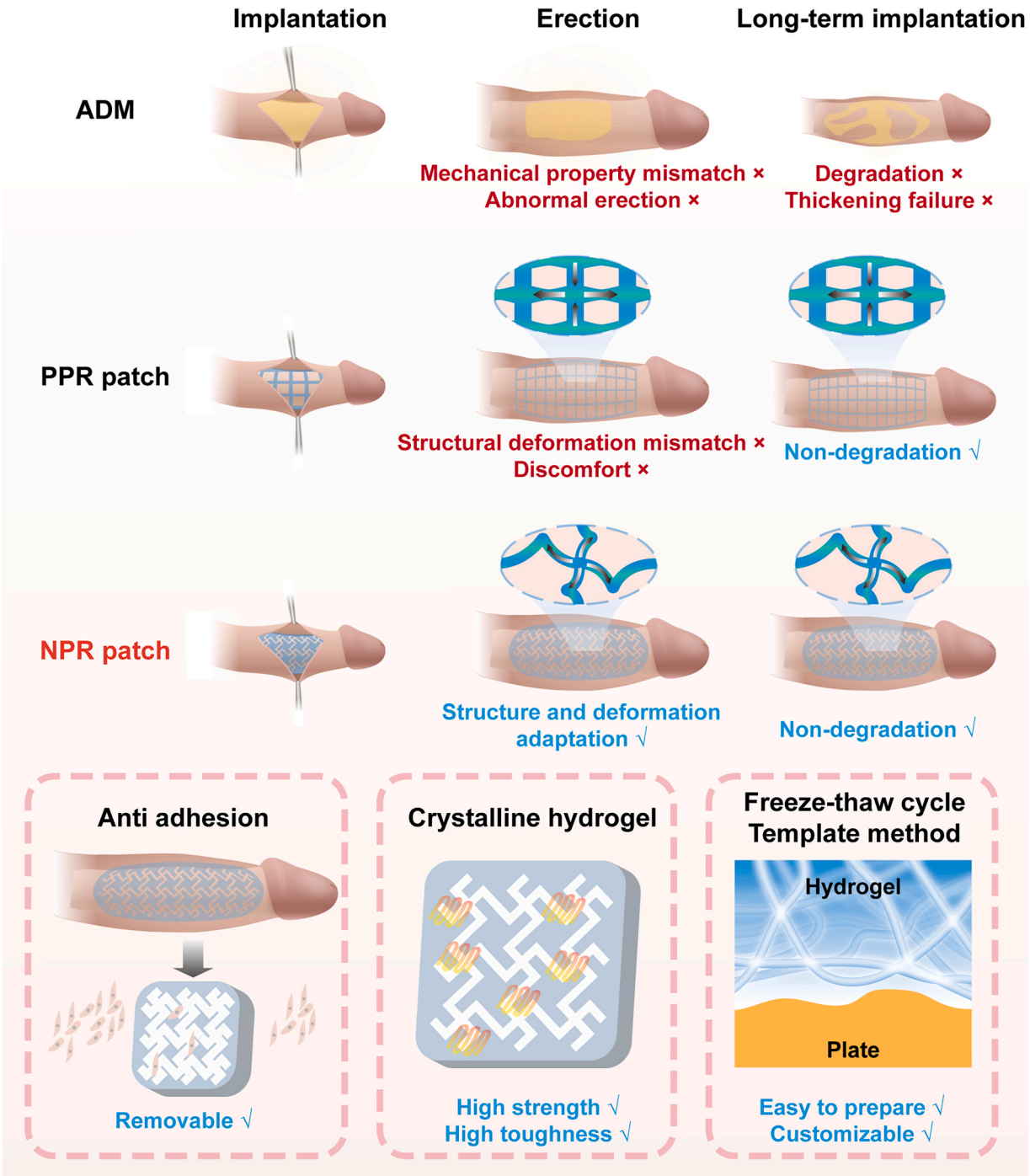

Fig. 1. Schematic representation of the penis enlargement effects achieved by the penis enlargement patches of different materials and structures. ADM is not compatible with the mechanical properties of the penis and could lead to abnormal erection. Long-term implantation is susceptible to degradation, resulting in failure to maintain increased girth. The structural deformation of the PPR patch was not in line with the natural deformation of the penis, potentially causing discomfort. Conversely, the deformation of the NPR patch was compatible with penile erection and did not degrade, thus ensuring a sustained enlargement effect. Additionally, the NPR patch has the ability to resist cell adhesion, making it easily removable. The crystallinity of the material was enhanced through alkali treatment, providing it with high strength and toughness. The NPR patch was prepared via a freeze–thaw cycle template method, enabling the customization to meet the individual needs.

penile augmentation implants includes autologous fat and an allogeneic dermal matrix[22–24]. While these methods have provided satisfactory augmentation in some patients, they can also cause serious adverse reactions. Notably, if an implant cannot be completely removed, potential side effects may occur, leading to prolonged patient suffering. To achieve long-term augmentation and minimize side effects, penile augmentation implant materials need to have stable mechanical properties and enable complete removal. Polyvinyl alcohol (PVA) is a processable hydrogel material with tunable mechanical properties, fatigue resistance[25–28], and high biocompatibility and has been widely used in biomedical applications such as vascular grafts [29], intraocular lenses [30], and artificial tunica albuginea [31]. Compared with those of other hydrogel materials such as hyaluronic acid, Due to their superior mechanical properties and nondegradable nature, PVA hydrogels are more suitable for use as penis enlargement patches.

Our research has been centered on the application of biomaterials in the field of reproductive medicine, with a particular focus on the repair of penile injuries. In our previous studies, we reported the use of 3D-printed hydrogel scaffolds for the reconstruction of injured corpus cavernosa [10], structurally biomimetic artificial tunica albuginea for functional replacement of the tunica albuginea [31], conductive hydrogels for the repair of cavernosal nerve injury (CNI) [32], and anti-inflammatory and antioxidant hydrogels for rapid re-epithelialization of the urethra [33]. In this study, we designed and constructed a penis enlargement patch with excellent compliance and long-term *in vivo* stability. To obtain a penile augmentation patch with a predefined structure, we introduced a PVA solution into a 3D printing mold and performed multiple freeze–thaw cycles. After the initial formation, the hydrogel patch was reinforced through an alkaline soaking process to ensure a precise match with the mechanical properties of the subcutaneous fascial tissue. To further achieve dynamic adaptation of the penile augmentation patch during the erectile process, we selected four typical NPR structures for optimization. Based on the structural utility from the construction with respect to the practical parameters, the chiral truss structure was identified as the optimal configuration, and this configuration was called the NPR patches; positive Poisson's ratio (PPR) patches and acellular dermal matrix (ADM) patches were used as control groups (Fig. 1). A series of *in vivo* and *in vitro* experiments demonstrated that the NPR patch possessed tissue-compatible mechanical properties, excellent biocompatibility, and antiadhesive properties and was capable of maintaining the penile augmentation effect for an extended period while minimizing side effects. This PVA hydrogel patch is not only applicable to penile enlargement surgery but also expected to be used for medical aesthetics and postsurgical reconstruction of other tissues, especially those requiring a dynamic microenvironment or long-term efficacy.

2. Results and Discussion

2.1. Preparation of alkali-treated enhanced PVA hydrogel patches

To achieve compatibility between the mechanical properties of a patch and penis, a hydrogel with improved mechanical properties needs to be developed. In accordance with the research of Darabi et al. [34], in this study, a method using an alkaline-reinforced PVA hydrogel was developed. This hydrogel was created by a series of freeze–thaw cycles, followed by immersion in sodium hydroxide (NaOH) to enhance its properties. The NaOH solution was subsequently removed via deionized water, resulting in a hydrogel suitable for penile enlargement applications. The manufacturing process was as follows: PVA, with a molecular weight of 146,000 to 196,000 Da, was heated and stirred to dissolve in 100 mL of deionized water. The patches were then subjected to several freeze–thaw cycles to form a PVA hydrogel. To further enhance the hydrogel, it was immersed in NaOH solutions of varying concentrations (4 M, 5 M, and 6 M). Upon completion of the enhancement process, the hydrogel was washed to remove any residual NaOH. The resulting hydrogels are denoted as xPVA-y, where "x" is the mass of PVA dissolved and "y" is the concentration of the immersion solution or NaOH used.

The processes of freeze–thaw cycling and subsequent alkali strengthening not only improve the structural integrity of the hydrogel but also tailor its mechanical properties to closely match those of the natural tissues that it is intended to augment. This matching of the mechanical properties is critical to the comfort and functionality of the patch when it is used. A photograph of the experimental results obtained by soaking different masses of freeze-thawed PVA hydrogels in different concentrations of NaOH solutions, ranging from 1 M to 6 M, is shown in Fig. S1. When PVA hydrogels are treated with low concentrations of NaOH (1 M–3 M), the enhancement effect is not significant. This is because the hydrogels retain a more transparent appearance, indicating that the crystallinity within the material is low. Higher crystallinity is often correlated with increased mechanical strength and stiffness [35]. However, in the context of this experiment, the low crystallinity resulting from treatment with low concentrations of NaOH indicates that the hydrogels were not sufficiently strengthened and that their mechanical properties were not markedly improved. On the basis of these observations, we decided to use higher concentrations of NaOH (4 M–6 M) for further experimentation.

The rheological properties of the PVA hydrogels were further investigated. In the linear region, the storage modulus (G') of the PVA hydrogels was always greater than the loss modulus (G''), indicating gel-dominant properties (Figs. S2–3). In contrast, both the G' and G'' of NaOH-treated hydrogels were greater than those of 15PVA-PBS, which indicated that the molecular chain movement of PVA was hindered by the NaOH treatment. The use of more concentrated NaOH solutions is expected to improve the crystallinity and consequently the mechanical properties of PVA hydrogels. The improvement of the mechanical properties is a critical step in the development process; the goal is to create a hydrogel with mechanical properties that are well matched to the requirements of penile tissue to ensure that the patch will be both effective and comfortable for its intended use. As shown in Fig. 2b and S4, 15PVA-5 M demonstrated the best mechanical properties. The tensile strength of 15PVA-5 M reached 3.01 MPa, and the elongation at break reached 299 %. Compared with human Buck's fascia [36], the 15PVA-5 M hydrogel has greater elongation at break and a lower modulus. As shown in Fig. 2c, according to the statistics of the 15PVA-PBS, its tensile modulus, elongation at break, tensile strength and toughness are 0.20 MPa, 152.67 %, 0.16 MPa and 35 kJ/m^2, respectively. After 15PVA-5 M was immersed in 5 M NaOH, its tensile modulus, elongation at break, tensile strength and toughness are 1.74 MPa, 299.07 %, 3.015 MPa and 3398.92 kJ/m^2; these values are 8.7, 2, 18.7 and 42.8 times greater than those of 15PVA-PBS, respectively. The cyclic stretching test results (Fig. 2d) demonstrated the remarkable durability of the hydrogel. After 1000 cycles of stretching, the hydrogel retained its original stretching characteristics, with negligible differences between the second and 1000th cycles. This consistent performance throughout the test period demonstrates the excellent fatigue resistance of the hydrogel; this resistance is a critical property for materials intended for long-term medical implantation, particularly in penile enlargement devices. In addition, based on its mechanical properties, the 15PVA-5 M hydrogel could support 500 times its own weight under various forms of mechanical stress, including twisting, curling, knotting, and stretching, without deformation (Fig. 2e). This robustness indicates that the hydrogel is not only suitable for penile enlargement but also has a high degree of versatility and reliability in terms of mechanical performance. The change in water content for different immersion times in 5 M NaOH is shown in Fig. S5. When the immersion time reached 6 h, no significant difference was observed in water content with continued immersion. Due to all of these properties, the hydrogel could adapt better to changes in shape and size during a penile erection while reducing the likelihood of fibrosis.

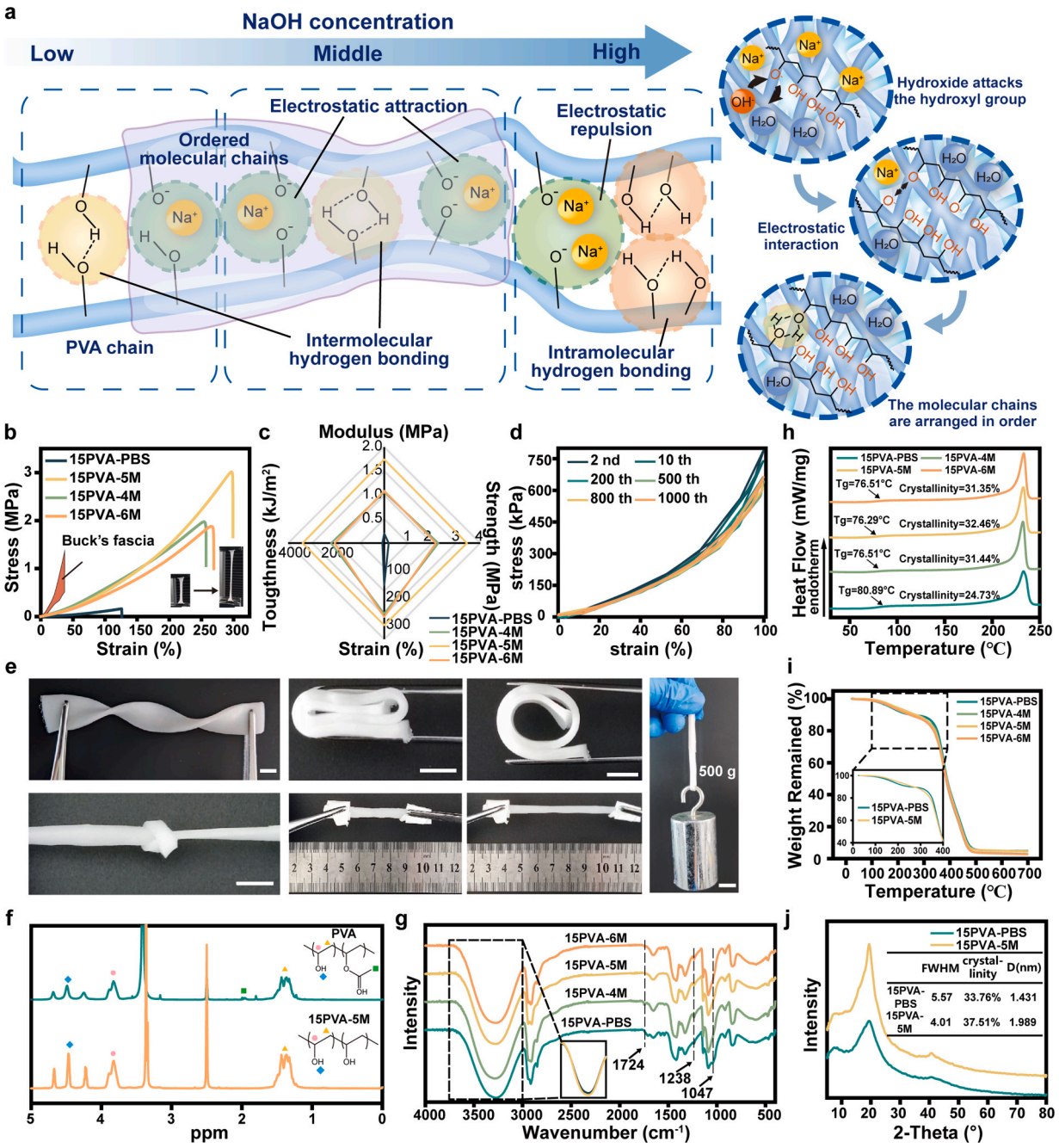

Fig. 2. Mechanical properties and mechanisms of patch exploration. a) Schematic diagram of the mechanism of PVA enhancement by NaOH. **b)** Uniaxial stretching curves of 5PVA-PBS, 15PVA-4 M, 15PVA-5 M and 15PVA-6 M and tensile mechanical properties of Buck's fascia [36]. **c)** Mechanical properties of the 15PVA-PBS, 15PVA-4 M, 15PVA-5 M and 15PVA-6 M hydrogels. **d)** Cyclic tensile curve of the 15PVA-5 M hydrogel. **e)** The 15PVA-5 M hydrogel; it can be twisted, folded, curled, knotted and stretched and is able to lift 500 times its weight without damage (scale bar: 1 cm). **f)** H^1-NMR spectra of the PVA particles and 15PVA-5 M hydrogels. **g)** ATR-FTIR, **h)** DSC and **i)** TG of 15PVA-PBS, 15PVA-4 M, 15PVA-5 M and 15PVA-6 M. **j)** XRD profiles of 15PVA-PBS and 15PVA-5 M.

2.2. Exploration of the enhancement mechanism

As shown in Fig. 2a, during the freeze–thaw cycle, the PVA solution underwent a transformation that improved its mechanical properties. The mechanism behind this enhancement involves the formation of ice crystals that extrude from the PVA molecular chains, creating cross-junction sites within the material. These cross-junction sites are critical to the formation of the crystalline regions within the hydrogel. When the PVA solution is soaked in NaOH, the hydroxide ions (OH^-) from the NaOH solution react with the hydroxyl groups present on the PVA molecular chains. Owing to their small size, free sodium ions (Na^+) in solution can easily penetrate the lattice of PVA molecular chains. These ions electrostatically interact with the oxide anions ($-O^-$), resulting in the formation of a stable complex structure. At lower concentrations of NaOH, such as 4 M and 5 M, the molecular chains are more likely to be drawn closer together by electrostatic attraction; this results in a more compact arrangement of the chains. After the Na^+ ions are washed away with deionized water, the resulting PVA hydrogel has a greater propensity to form crystalline zones and intermolecular hydrogen bonds. This is due to the more regular alignment of the molecular chains, which facilitates the formation of a stable and robust network. However, as the concentration of NaOH increases, more hydroxyl groups on the PVA chains are attacked by the OH^- ions, and more oxide anions are formed. Each of these oxygen atoms attracts one Na^+ ion. Owing to the limited

space between the molecular chains, the presence of two opposing Na^+ ions can lead to electrostatic repulsion, increasing the distance between the molecular chains. Once the Na^+ ions are removed by washing with deionized water, the increased distance between the chains causes difficulty for the formation of the intermolecular hydrogen bonds. Instead, intramolecular hydrogen bonding becomes more prevalent, resulting in a sparser arrangement of the chains within the intermolecular lattice. This decrease in the intermolecular interactions can affect the mechanical properties of the hydrogel, resulting in a less dense and more flexible structure. The surface contact angle results are shown in Fig. S6. Compared with that of 15PVA-PBS, the hydrophilicity of the surface increased after NaOH treatment. This further indicates that NaOH treatment increases the number of exposed hydroxyl groups and that the molecular chains are more flexible; these conditions are favorable for the formation of crystals. After treatment with higher NaOH concentrations, intramolecular bonds are more easily formed than intermolecular hydrogen bonds. The intramolecular hydrogen bonds travel through a stable six-membered ring system, which is difficult to break, whereas hydrogen bonding is saturated, and fewer hydroxyls can be formed, resulting in lower hydrophilicity and a larger contact angle.

The analysis of the PVA polymer backbone modifications via various spectroscopic and analytical techniques provides a comprehensive understanding of the structural and chemical changes that occur upon treatment with NaOH. The proton nuclear magnetic resonance (H^1-NMR) spectra (Fig. 2f) reveal that NaOH attacks the acetate group on the PVA backbone, leading to hydrolysis of the ester group. This reaction results in the introduction of more hydroxyl groups along the polymer chain, which increases the flexibility of the PVA backbone. This enhanced flexibility is beneficial for the mechanical properties of the PVA hydrogel, as it allows for better adaptation to stress and strain. The Fourier transform infrared (FTIR) spectra (Fig. 2g), particularly in the range of 3600–3000 cm^{-1}, show an increase in the intensity and width of the absorption peaks after NaOH treatment. This increase is attributed to the strengthened hydrogen bonding interactions within the polymer matrix. The specific peaks at 1724 cm^{-1} (C=O stretching vibration in the ester group) and 1238 cm^{-1} (C-O stretching vibration in the PVA chain) are indicative of these interactions. The prominent peak at 1047 cm^{-1} corresponds to the C-O stretching vibration in the ester group and is also associated with the O-C-C inverse stretching vibration or the amorphous peak of PVA. The prominent peak observed in the 15PVA-6 M sample indicates a decrease in the degree of crystallinity, with a more amorphous and flexible structure. The differential scanning calorimetry (DSC) results (Fig. 2h) reveal that after treatment with NaOH, the degree of crystallinity increases, and the highest crystallinity is observed after treatment with 5 M NaOH. Concurrently, the glass transition temperature (T_g) decreases to a certain degree, and the lowest T_g is observed after treatment with 5 M NaOH. This result indirectly confirms that the PVA hydrogel exhibits the highest degree of crystallinity following treatment with 5 M NaOH. TGA (Fig. 2i) analysis reveals a slope change in the first region due to water evaporation; this is slightly hindered by changes in the crystal structure of PVA after alkali treatment. The second region of weight loss is primarily caused by the breakage of hydrogen bonds and the degradation of the PVA backbone. Without alkali treatment, the molecular chains are entangled; thus, they need to be untangled before degradation can occur. In contrast, after NaOH treatment, the molecular chains are aligned, reducing the energy required for material degradation [34]. The X-ray diffraction (XRD) results (Fig. 2j) confirm the increase in crystallinity after NaOH treatment, as calculated on the basis of the peak area. The use of Scherrer's formula (**Equation (1)**) to calculate the grain size indicates that the grain size increases. This further supports the concept that the molecular chains are arranged more tightly and that the crystallization area is larger after the removal of NaOH. In summary, the treatment of PVA with NaOH results in significant structural changes that enhance the mechanical properties and flexibility of the polymer.

$$D = \frac{K\gamma}{B\cos\theta} \quad \text{(Equation 1)}$$

Here, D is the average thickness of the grain perpendicular to the direction of the grain surface (Å), B is the half-height width of the diffraction peak of the measured sample, and K is Scherrer's constant; when B is the half-height width of the diffraction peak, then K = 0.89. θ is the Bragg diffraction angle, and γ is the wavelength of the X-rays.

Tensile tests were performed on PVA materials with different types and concentrations of alkali. As shown in Fig. S7, the promotion of PVA crystallization by LiOH is limited at concentrations above 5 M due to its solubility limitations. The K^+ ions have difficulty penetrating the PVA crystal lattice due to their larger size; thus, the promotion at lower concentrations is achieved mainly by the action of OH^-, which leads to a more ordered arrangement of the PVA molecular chains. However, as the concentration continues to increase, the cations have a declining synergistic effect on the molecular chains, resulting in limited enhancement. With further increases in concentration, the cations have great difficulty attaining further synergistic effects on the molecular chains, which also limits the enhancement potential of the material.

2.3. Optimization of the penis enlargement patch structure

The prepared patches typically exhibit a positive Poisson's ratio, whereas the transition of the penis from flaccid to erect demonstrates an NPR with increasing girth as the length increases. According to the literature[37–39], the penis possesses an NPR, with the erect circumference being approximately 150 % of the flaccid circumference and the erect length being approximately 125 % of the flaccid length. On the basis of this understanding, four structures with NPR characteristics were designed, as shown in Fig. 3a: re-entrant honeycomb (REH), orthogonal oval void (OOV), chiral truss (CT), and star-shaped (SS) structures. In addition, two common structures were constructed: rectangular (R) and honeycomb (H) structures. For these six different structures, parameters such as height (h), width (w), thickness (t), and angle (α) were designed (the thickness in the z-axis direction was 5 mm), and computational modeling and experimental validation were carried out. The models were fitted via the Mooney–Rivlin hyperelastic material model with two parameters. The tensile data of the measured 15PVA-5 M sample were imported into the fitting model. The two-parameter results obtained from the fitting were C01 = 2.0270e5 and C10 = 1.7535e5. For the mechanical studies, these fitting parameters were then incorporated into the hyperelastic material model, and a transient uniaxial tensile simulation was conducted via COMSOL Multiphysics. The simulation conditions were set to stretch to 60 % of the original length, which more closely aligned with practical application scenarios. The designed patches also had different sizes and numbers of repeating units because of the different demands facing individuals. Therefore, different structures were randomly selected, and patches with different numbers of repetition units were designed, as shown in Fig. S8. For structural mechanical simulation, the patches of these structures were imported into COMSOL Multiphysics 5.6, and the resulting mechanical properties are shown in Fig. 3b. The structural mechanical properties of the patches with different numbers of repeating units were similar; therefore, to reduce the computation time and computational resource consumption, most of the structures selected for simulation consisted of a small number of repeating units (3 × 3 or 5 × 5).

Uniaxial tensile simulations were performed for each structure, and the results of the obtained von Mises stress diagrams are shown in Fig. 3c; specifically, the R and H structures clearly did not exhibit NPR properties. During the stretching process, the main stress-bearing areas of the R structure were parallel to the direction of stretching, whereas the stress concentration in the H structure was shown at the corners of the hexagons. When stretched, the PPR structures had difficulty experiencing structural deformation. Compared with a complete patch, the PPR structure is characterized by high porosity; this results in the stress

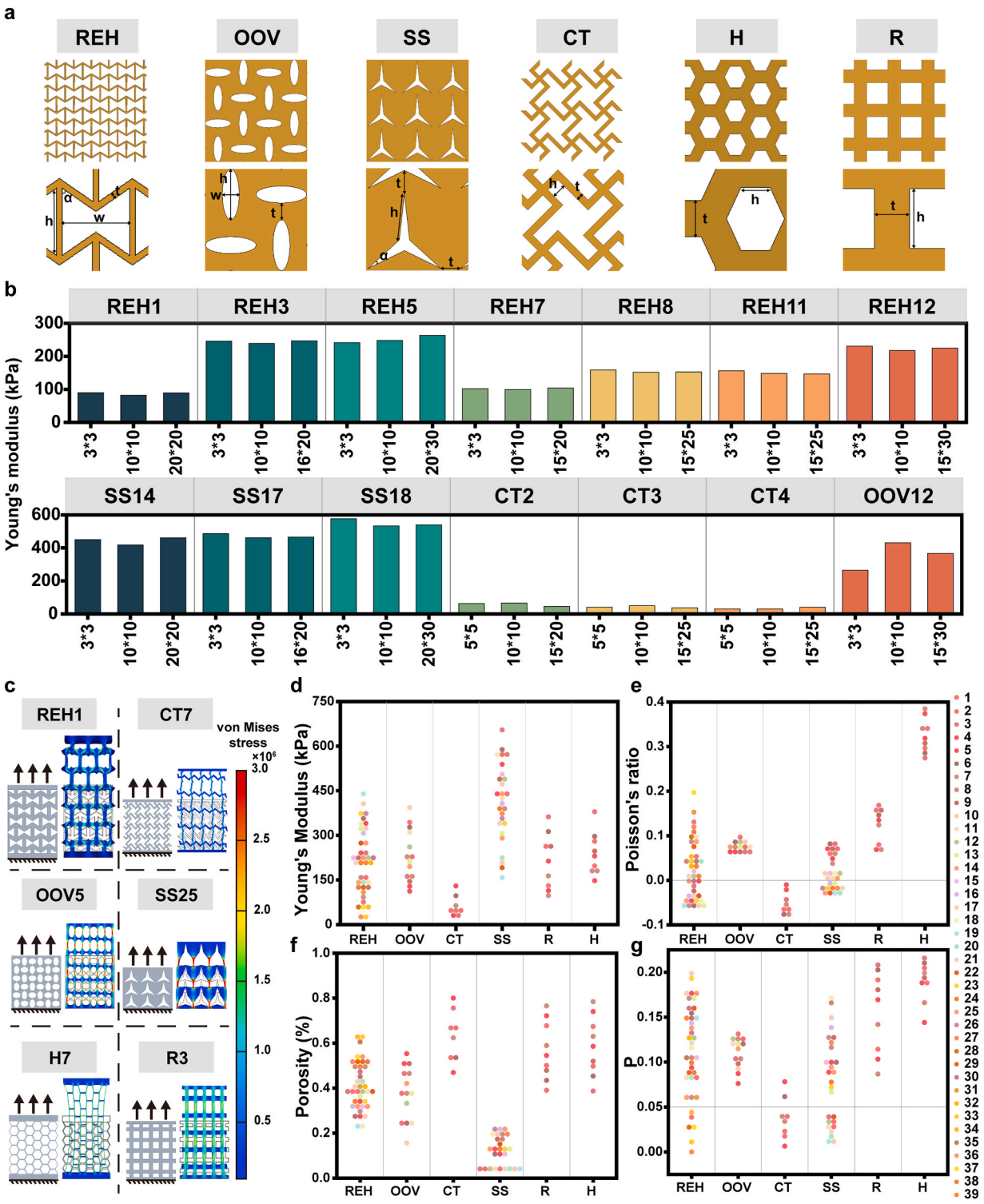

Fig. 3. Patch design and computational simulation: a) Structural characteristics and parametric design of each patch; **b)** mechanical properties of the structures with different numbers of repeating units; **c)** von Mises stress of various types of structures; different structural patches are quantitatively evaluated for each structure via computational simulations of **d)** Young's modulus and **e)** Poisson's ratio under 60 % stretching; **f)** porosity for different structural designs; and **g)** definition of the practicality parameter P is defined. When $P \leq 0.05$, the structure is determined to be suitable for penile thickening.

concentration being located in the area parallel to the stretching direction. During stretching, the OOV structure also did not demonstrate NPR behavior. This could be due to the considered material properties; as the structure was stretched, the material itself was also stretched, and the material deformation exceeded the structural deformation, which would otherwise contribute to the NPR. Additionally, the stress distribution maps indicated a marked stress concentration at the connections of the OOV structure, and these stresses could lead to defects and patch failure in practical use. The SS structure exhibited certain NPR properties. As the stretching process progressed, the SS structure gradually deformed, and the main areas of deformation occurred in the regions where the material was stretched, leading to severe stress concentration. However,

the REH and CT structures clearly exhibited NPR properties during stretching, and the stress distribution maps showed no significant stress concentration defects. This was attributed to the well-designed structure, in which the structural deformation and material deformation worked in conjunction during the stretching process. The structural deformation helped to mitigate stress concentration defects to a certain extent. Furthermore, the porous structure of the NPR Penile Enlargement Patch may facilitate the growth of subcutaneous loose connective tissue to a greater extent than an intact sheet structure. This may result in enhanced tissue integration and a reduced risk of displacement following implantation.

To ensure compatibility with the physiological changes in the penis, the engineered structure needs to exhibit a reduced elastic modulus and a suitable negative value for the Poisson's ratio. A lower elastic modulus

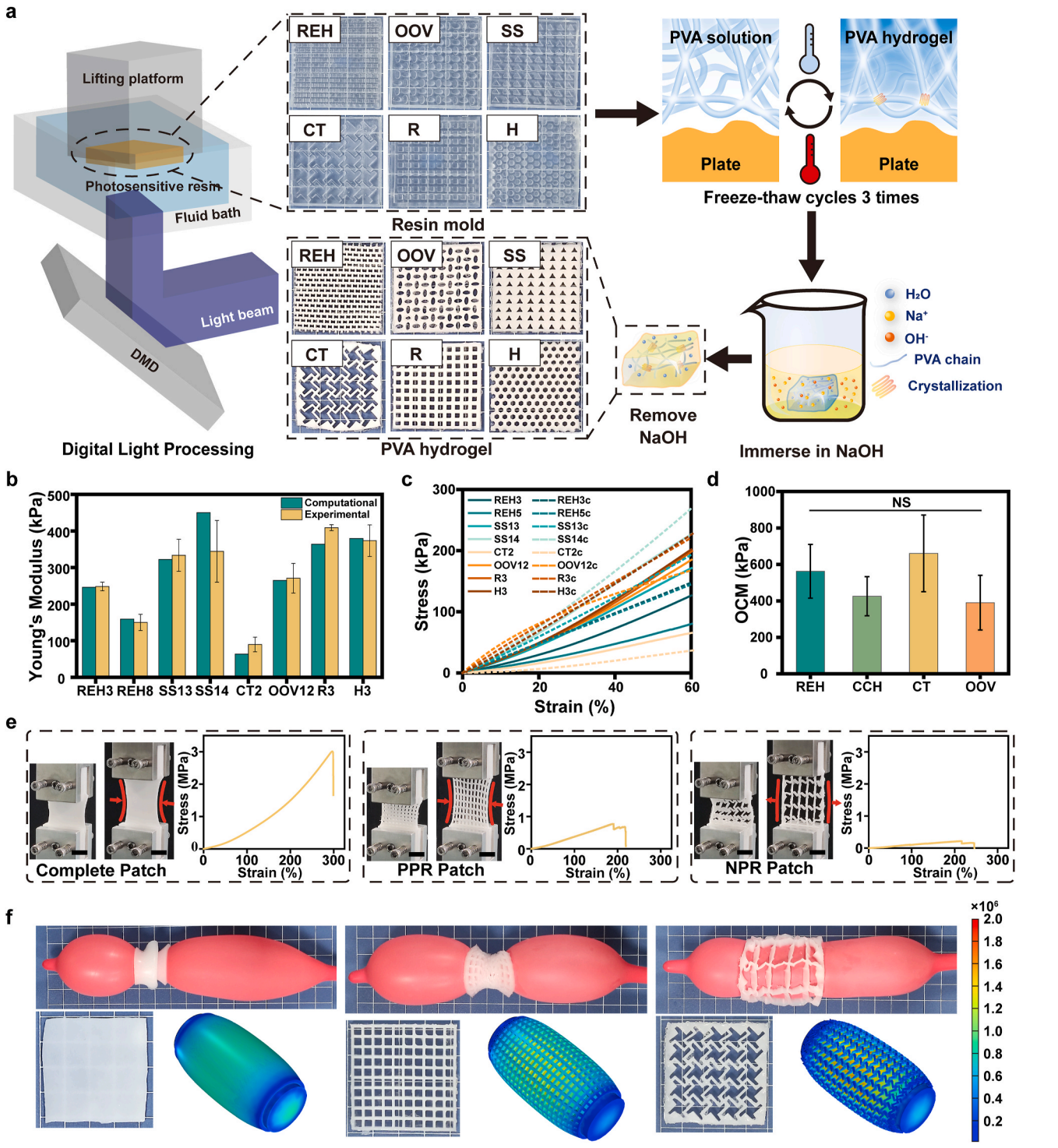

Fig. 4. Preparation and *in vitro* model validation of a patch for penile enlargement. a) Schematic of the structure of the penis enlargement patch, and digital photos of the mold and the hydrogel patch. Comparison of the simulated and actual test results for **b)** Young's modulus and **c)** tensile curves. **d)** Overall compression modulus of the NPR patches with different structures. **e)** Tensile test digital photos (scale bar: 1 cm) and mechanical properties of the different patches. **f)** Physical and mock-up images of a balloon model simulating penile deformation (complete patch, R structure and CT structure patch). ($n \geq 3$, NS = not significant).

helps alleviate stress on the penis during erection, whereas a properly chosen NPR enhances the natural aesthetics of the penis in its erect state. The simulation outcomes were subjected to a statistical evaluation to determine the values of the Young's modulus (Fig. 3d), Poisson's ratio (Fig. 3e) and porosity (Fig. 3f), and Poisson's ratio is computed according to the formula presented in **Equation (2)**:

$$v = -\frac{\Delta x}{\Delta y} \quad \text{(Equation 2)}$$

where Δx is the deformation in the x-direction and Δy is the deformation in the y-direction.

A strong correlation is observed between the mechanical characteristics of the R structure and H structure and their respective edge thicknesses, which in turn influences the modulus distribution. The H structure, when deformed, clearly demonstrates a PPR, meaning that it tends to contract laterally when stretched. Similarly, the mechanical properties of OOV and SS structures are also generally stronger, and these stronger properties are related to the site of stress concentration in their design. In addition, the design of structures with smaller spacings and stress concentrations leads to weaker mechanical properties; in the case of the OOV structure, its stretching by 60 % results in an insufficient ellipse deformation, and the material deformation is predominant and prevents the structure from exhibiting an NPR. The deformation of the SS structure is influenced by the specific design parameters; a smaller angle α and reduced spacing t enhance the structure's NPR, which is characterized by lateral expansion during stretching, but this intensifies the stress concentration issues. The mechanical strength of the REH structure is notably diverse, and the variability in its Poisson's ratio is contingent on the selected structural parameters. An increase in the spacing t leads to enhanced mechanical properties, whereas the angle α affects mainly its negative Poisson's ratio properties. Finally, the CT structure is characterized by a generally low modulus, which is closely related to its high porosity; since all variations feature an NPR, the CT structure is the most suitable option for scenarios where such mechanical properties are desirable.

To quantitatively assess the practicality of each structure and compare different structures, a dimensionless practicality parameter P is defined (as shown in **Equation (3)**):

$$P = Nor(modulus) \cdot Porosity \quad \text{(Equation 3a)}$$

where Nor (modulus) is the normalized modulus (the modulus removes the maximum and minimum values).

The results obtained are shown in Fig. 3g. When $P \leq 0.05$ is defined as a structure adaptable for penile enlargement, some of the REH and SS structures and the vast majority of the CT structures met the requirements for use.

As shown in Fig. 4a, we used 3D printing to create molds on the basis of the structural design. The molds were then filled with the PVA solution, freeze–thaw cycled three times and then reinforced with NaOH to prepare 15PVA-5 M patches with a certain structure. We conducted both tensile and compression tests on these patches and compared the outcomes of the tensile tests with the Young's modulus values derived from theoretical computations. The comparative results are illustrated in Fig. 4b, demonstrating a minimal discrepancy between the theoretical and actual tensile moduli. This close correlation indicates that the theoretical models provide valuable insights for reference. Upon juxtaposing the theoretical curves with the empirical data, as presented in Fig. 4c, the majority of the curves effectively align with each other. To investigate the relationship between the compressive properties and porosity of the patch, the overall compressive modulus (OCM) was defined as shown in **Equation (3)**:

$$OCM = \frac{E}{1-\varphi} \quad \text{(Equation 3b)}$$

where E is the compression modulus of the patch and φ is the porosity of the patch.

As shown in Fig. 4d, no significant difference is observed between the OCMs of different types of structures; thus, the porosity likely affects the compression performance of the patch over the structural design.

The digital images (Fig. 4e) captured during the stretching process reveal that the complete patch and h structure lack the NPR trait, whereas the structure engineered to exhibit an NPR clearly undergoes a noticeable change in the x-direction during stretching. The tensile curves of the various types of patches are shown in Fig. 4e; here, the patches with structures are weaker than the complete patch due to the increase in porosity. However, the NPR patch has a weaker Young's modulus and greater elongation at break than the PPR patch does and is attributed to the structural design; these results indicate that the NPR structure is superior to the orthogonal mesh structure. A comparison of the CT structure before and after stretching is shown in Fig. S9 and reveals that the middle structure can still maintain its original shape after 1000 cycles of stretching. Its tensile stress–strain curve is shown in Fig. S10, which reveals that the CT structure has a certain stability and does not fail after 1000 cycles. To emulate the variations in the penis size, a balloon filled with water served as an analog. The patch was affixed to the balloon surface, and the balloon was incrementally filled with a certain amount of water to mimic penis enlargement. As shown in Fig. 4f, the incorporation of an NPR patch does not adversely affect the erection process of the "simulated penis". On the other hand, the use of the complete patch and PPR patch leads to irregular erections in the "simulated penis": these results indicate the potential for stress concentration post-implantation, which could subsequently cause patient discomfort. To further investigate this, a balloon-in-water model was developed via COMSOL Multiphysics to simulate the conditions of a penile erection. The von Mises stress distribution within this model reveals a stark contrast between the different patch types. The complete patch and PPR patch have high levels of stress concentration in their exteriors. In contrast, when the NPR patch is subjected to external forces, the structural deformation relieves the stress concentration caused by material deformation to a certain extent, and no significant stress concentration is observed. This disparity in the stress distribution is crucial because it directly influences the comfort and functionality of the implant. High stress concentrations can lead to localized pressure and potential discomfort or even injury to the surrounding tissue. Therefore, due to its uniform stress distribution, the NPR patch is a more viable option for penile enlargement applications. *In vitro* modeling tests further supported the superiority of the NPR patch over the complete patch and the PPR patch in terms of penile enlargement. These tests validated the computational findings, confirming that the NPR patch is better equipped to handle the mechanical demands of penile enlargement without compromising patient comfort. In essence, the NPR patch emerges as the optimal choice for penile enlargement because of its ability to maintain a natural erection process in the "simulated penis" and its reduced stress concentration profile. This innovative design ensures a more comfortable and effective penile enlargement solution, as evidenced by both computational simulations and *in vitro* testing.

2.4. *In vivo/in vitro* biology of penis enlargement patches

The biocompatibility of the hydrogels was thoroughly investigated to determine their suitability for clinical use. The focus of this study was on four specific hydrogels: 15PVA-PBS, 15PVA-4 M, 15PVA-5 M, and 15PVA-6 M. The surface morphology of the lyophilized hydrogels was observed by using scanning electron microscopy (SEM), as shown in Fig. S11; here, the PVA hydrogels had a porous structure suitable for cell growth both before and after NaOH treatment. The cytotoxicity of these hydrogels was assessed via the Cell Counting Kit-8 (CCK-8) assay and live/dead staining assay [40,41], and the findings are shown in Figs. S12–13. These results suggest that the hydrogels have minimal cytotoxic effects. The anti-protein and cell adhesion properties of the 15PVA-PBS and 15PVA-5 M hydrogels were subsequently evaluated

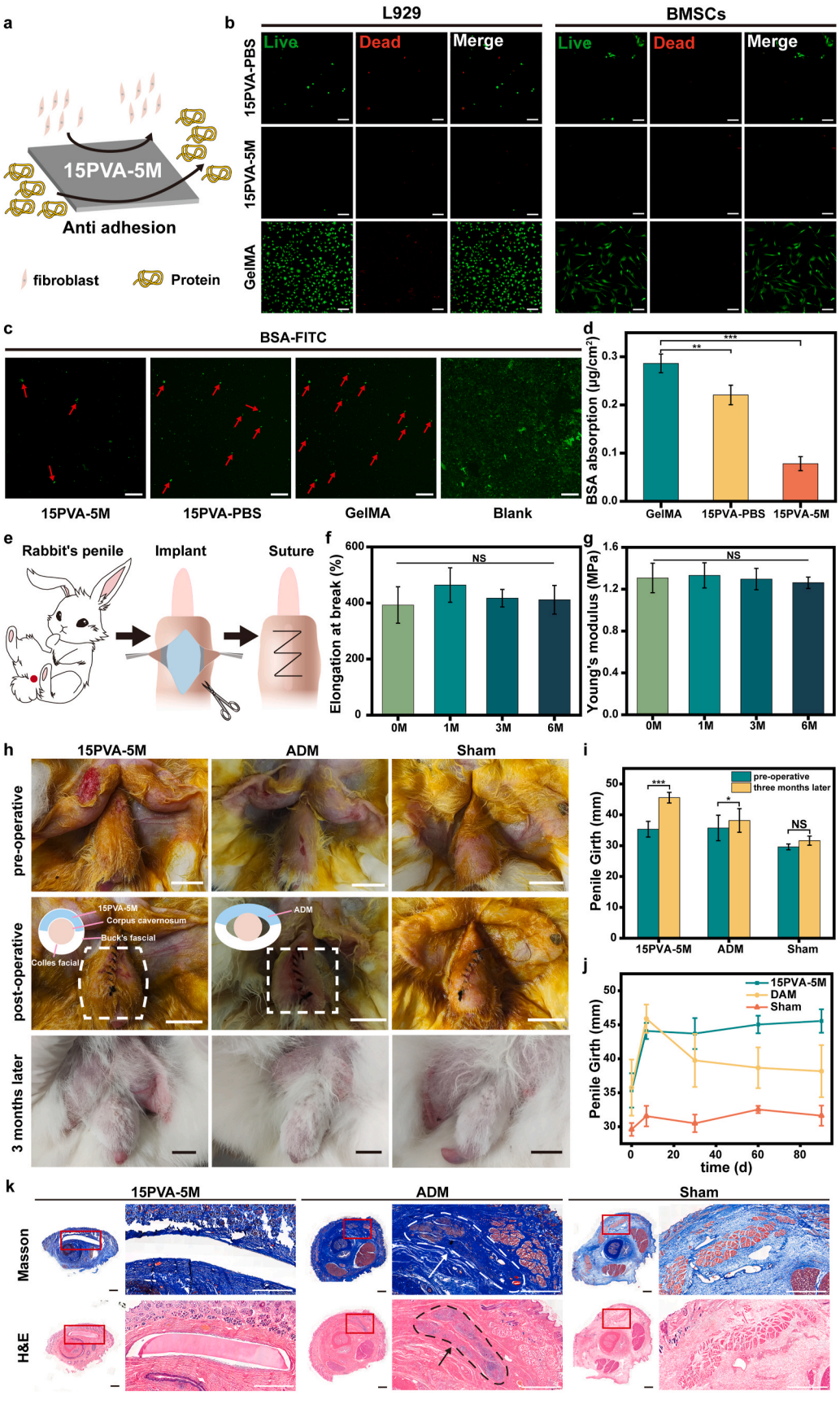

(caption on next page)

Fig. 5. Biocompatibility testing. a) Schematic diagram of the effects of the 15PVA-5 M hydrogel on cell adhesion and protein adhesion. **b)** Cell adhesion fluorescence image (scale bar: 100 μm) of 15PVA-5 M, 15PVA-PBS and GelMA. **c)** Protein adhesion fluorescence image (scale bar: 100 μm). **d)** Quantitative protein adhesion content test. **e)** Schematic diagram of the animal experiment process. **f)** Young's modulus and **g)** elongation at break of the 15PVA-5 M hydrogel soaked for 6 months. **h)** Digital photos of a rabbit penis (before surgery, after surgery and three months after surgery) (scale bar: 1 cm). **i)** Comparison of the penile girth in rabbits before and three months after surgery. **j)** Changes in the penile girth over time in rabbits. **k)** Representative microscopy images (scale bar: 2 mm) of the penile cross sections stained with Masson's trichrome and H&E. ($n \geq 3$, *$p < 0.05$, **$p < 0.01$, ***$p < 0.001$. NS=Not significant).

(Fig. 5a). As shown in Fig. 5b, both types of cells adhered less to the 15PVA-5 M hydrogel, indicating that the penile enlargement patch has good anti-cell adhesion properties, which aids in postoperative removal and does not easily lead to fibrosis. The adherence of BSA-FITC to the samples was examined via laser confocal microscopy, and the images are shown in Fig. 5c. In addition, quantitative analysis was performed via a bicinchoninic acid (BCA) assay kit, and the results are shown in Fig. 5d. Notably, the 15PVA-5 M hydrogel showed better antiadhesion to cells and nonspecific proteins than the control group, which in this case was GelMA.

First, *in vitro* experiments were conducted to evaluate the durability and mechanical stability of the hydrogel over time. The 15PVA-5 M hydrogel was submerged in phosphate buffered saline (PBS) for six months to evaluate any changes in its tensile properties. The results of this long-term immersion test are presented in Fig. 5f–g. No significant alteration was observed in Young's modulus or the elongation at break of the hydrogel after six months; these results strongly indicated that the 15PVA-5 M hydrogel was capable of retaining its mechanical integrity during prolonged implantation periods. *In vivo* implantation studies were conducted in New Zealand rabbits to evaluate the suitability of two different materials for penile enhancement (Fig. 5e). Compared with rats, rabbits have a larger penis; thus, the surgery can be more easily performed, and the absence of a penile bone in rabbits is more compatible with the structure of the human penis than it is in larger animals. The surgical intervention involved a direct incision of the penile skin, revealing the underlying deep fascia, followed by the insertion of the study materials ADM and 15PVA-5 M hydrogel. A sham surgery group was also established for comparative analysis. Post-implantation observations (Fig. 5h) indicated that the 15PVA-5 M hydrogel integrated more seamlessly with the penile skin. This was attributed to its mechanical properties, which are more similar to those of the penis, as opposed to those of the ADM. Owing to its more robust mechanical properties, ADM tended to slightly lift the penile skin, which could lead to a sensation of a foreign body. Photographic documentation taken after 3 months revealed that the experimental group (15PVA-5 M) maintained significant thickening of the penile tissue. In contrast, the control group, which underwent sham surgery, showed no significant changes in their penile appearances. The surgical removal of 15PVA-5 M is shown in Fig. S14, and vascular growth was observed on the patch; thus, 15PVA-5 M had good biocompatibility. A comparison of penile diameters before and after implantation (at three months) (Fig. 5i) confirmed that the 15PVA-5 M hydrogel effectively increased penile girth. Furthermore, an analysis of penile circumference over time (Fig. 5j) revealed that the 15PVA-5 M hydrogel exhibited a consistent thickening effect throughout the study period. In contrast, ADM began to degrade over time, resulting in a decrease in the initial thickening effect. As shown in Fig. S15, erection photographs of the rabbits were taken three months after implantation. When the experimental group was compared with the control group and the blank group, the implantation of the patch did not affect the rabbits' penile erection and did not lead to abnormal penile erection. Based on these results, the 15PVA-5 M hydrogel is a promising material for penile enhancement because of its biocompatibility and ability to maintain a stable thickening effect over time.

Three months later, the penises of three groups of New Zealand rabbits were sampled, embedded in sections, and stained with Masson's trichrome and H&E. The staining results are shown in Fig. 5k. The implanted material in the ADM group underwent significant degradation, as indicated by the arrows in Fig. 5k. The degradation products were absorbed by the penis, resulting in a darker color on Masson's trichrome staining. Thus, the basic function of thickening was difficult to maintain. Additionally, a slight inflammatory reaction at the implantation site was observed. No discernible fibrosis or inflammatory reaction was found near the implant in the 15PVA-5 M group, and the degree of fibrosis was comparable to that observed in the sham-operated group. Figs. S16–18 show the blood counts and pathological sections of the heart, liver, lungs, kidneys, and testes. These data showed that the implantation of 15PVA-5 M did not result in any significant systemic toxicity or an inflammatory response. Therefore, 15PVA-5 M is a promising penile thickening patch for clinical application.

PVA hydrogels were prepared via a simple template method and freeze–thaw cycle method. They were subsequently enhanced by immersion in NaOH for the preparation of the patches with an NPR structure for penile thickening. Experimentally, 15PVA-5 M exhibited optimal mechanical properties. Scoring criteria were developed for different structures, and the CT structure was found to be the optimal structure, better adapting to the erectile and flaccid deformations of the penis. However, several limitations are present. In particular, (1) rabbits do not exhibit evident self-injurious behaviors (e.g., biting and devouring the penis), and they are unable to express intuitive sensations such as those of humans; therefore, the comfort and foreign body sensation of the implant need to be further evaluated; (2) the structure of a rabbit penis is different from that of a human penis. When a rabbit penis is erect, the outer epidermis changes less as the penis thickens. Implantation of the patch in a rabbit penis does not accurately mimic the changes in erection and weakness of a human penis; and (3) genotoxicity testing of implantable materials for medical devices is lacking. Genotoxicity testing is essential to confirm the safety and reliability of an implant if it is to be used clinically for penile enlargement. Future clinical trials are needed to demonstrate the feasibility of the penis thickening patch. We will optimize the experimental protocol in the future to realize the clinical application of penis enlargement patches.

3. Conclusion

In this study, we developed a novel penis enlargement patch, designated 15PVA-5 M, via a template-based method to design structures with adjustable NPRs. This innovative approach, complemented by NaOH treatment, resulted in a patch with superior mechanical strength. Through careful finite element analysis, we optimized the design to mimic the natural deformation behavior of the penis. Incorporating an NPR into the patch architecture effectively reduced its stiffness, minimizing the stress placed on the penis during post-implantation deformation. Initial *in vitro* evaluations demonstrated the biocompatibility of 15PVA-5 M. Subsequent *in vivo* studies using a rabbit penile implant model demonstrated that the patch was resistant to degradation and fibrosis over time, maintained its structural integrity and consistently provided the desired penile augmentation. Considering the anatomical differences between rabbits and humans, further investigation of the device is essential for a more comprehensive assessment of the patch's clinical viability. The customizable molds utilized in the manufacturing process permit enlargement patches to be employed for a multitude of medical and cosmetic purposes, in addition to penis enlargement. Furthermore, they are suitable for the reconstruction of various tissues and organs following surgical removal of tumors or injuries.

4. Experimental section

4.1. Preparation of NaOH-enhanced PVA hydrogels

First, 10 g, 12.5 g and 15 g of PVA granules (Sigma–Aldrich, molecular weight 146000–186000 Da, degree of hydrolysis 99 %) were weighed, added to 100 mL of deionized water, heated to 90 °C and stirred vigorously. After complete dissolution, the material was loaded into Petri dishes, frozen at −20 °C for 12 h, and thawed at room temperature for 4 h; this process was repeated three times to obtain the PVA hydrogels. A cutter was used to cut the dumbbell-shaped samples and disks in preparation for the subsequent testing. The PVA hydrogels obtained from these cuttings were soaked in PBS and NaOH solutions (at concentrations of 1 M, 2 M, 3 M, 4 M, 5 M, and 6 M) and then soaked in deionized water to wash away NaOH; the resulting hydrogel was named xPVA-y where x denotes the mass of PVA, and y denotes the soaking solution.

4.2. Preparation of the PVA hydrogel patches with a negative Poisson's ratio

The molds were prepared via a digital light processing (DLP) printer (Bio-Architect PR, Regenovo Biotechnology Co. Ltd., China) to print photosensitive resins (esun, PM200 PMMA-Like Resin), and a total of six types of structures were designed (see Results and Discussion for details). The size of the mold was approximately 50 mm × 50 mm × 5 mm, and the depth of the groove was 5 mm. The PVA solution was loaded into the mold, freeze-thawed 3 times, and immersed in NaOH at a concentration of 5 M, and patches with the designed structure were obtained by washing away the NaOH solution.

4.3. Mechanical tests

Dumbbell-shaped samples (the thickness of the test section was approximately 1.5 mm, and the length was approximately 20 mm) were loaded into a universal mechanical testing machine (Instron 5967, Instron Corporation, USA) and subjected to uniaxial tensile testing at a speed of 40 mm/min. Similarly, cylindrical samples with a diameter of approximately 5 mm and a height of approximately 8 mm were loaded into a universal testing machine for uniaxial compression tests at an experimental speed of 1 mm/min. Next, cyclic tensile tests were performed using the dumbbell-shaped samples (the test section thickness was approximately 1.5 mm, and the length was approximately 20 mm) loaded into a universal testing machine with a deformation rate of 400 %/min for 1000 cycles.

4.4. Patch design

These patches were designed in Creo 6.0 software. The repeating cells of the patch are first designed (as shown in Fig. 3a), and then multiple repeating elements are generated in the x- and y-directions. The different parameters in the patch (Table S1) are assigned to global variables, and patches with different properties are obtained by adjusting the variables. To facilitate subsequent simulations and practical experiments, rectangular blocks are designed at both ends of the patch.

4.5. Finite element simulation

The computational modeling was performed using the structural mechanics module of COMSOL Multiphysics 5.6 with a transient simulation. First, the material parameters were fitted. Owing to the properties of the PVA hydrogel with the hyperelastic material model, the mechanical properties of the PVA hydrogel obtained from the actual tests were fitted via the Mooeny–Rivlin two-parameter model, and the expressions for the fitted parameters, C10 and C01, are shown in Equation (4):

$$P = 2 * (C10 + C01 / lambda) * (lambda - 1 / lambd\hat{a}2) \quad \text{(Equation 4)}$$

where P is the engineering stress and lambda is the shape variable. The nature of the superelastic material of the patch is described as follows: the fixed constraint is set at one end, the other end is subjected to transient simulation, and the moving speed is set to 40 mm/min (corresponding to the actual test). To save computing resources during the simulation, a 3 × 3 structure is used. To match the actual situation, the deformation variable is stopped at 60 %, the pressure and x-direction displacement at the center position of the patch are calculated; afterward, Young's modulus and Poisson's ratio are calculated.

4.6. Multicell patch simulation

For further fitting to the actual use case, the patches with different numbers of cells were designed via Creo 6.0, as shown in Fig. S4, and the style modulus obtained from the fitting was compared with that of the 3 × 3 structural cell patch.

4.7. Penile erection simulation

Penile erection was simulated via a simplified balloon injection model. The cavity cylinders were designed with Creo 6.0, and patches of different structures were designed to wrap around the cylinder surface. The simulations were performed using the COMSOL Multiphysics 5.6 structural mechanics module; the water injection was set to 1.5 times the internal volume of the cavity to observe the stress concentration.

4.8. In vitro simulation balloon model

A long strip of balloon with a mass of approximately 1.8 g was filled with water to simulate the deformation of a penis. The balloon was filled with 200 mL of water, and the end was clamped with a dovetail clip to prevent leakage. Owing to the poor mechanical properties of the water-filled balloon, an unreinforced PVA patch was used for wrapping, and the patch was secured via a surgical suture (Shanghai Tianqing Biomaterials Co., Nonabsorbable Surgical Suture, 3-0) wrapped around the surface of the balloon.

4.9. Animal experimentation

Nine 2.5 kg–3 kg New Zealand male rabbits were purchased from Huadong Xinhua Experimental Animal Breeding Farm in Huadu District, Guangzhou city, and were randomly divided into three groups: the control group (ADM-implanted), the sham-operated group and the experimental group. The New Zealand male rabbits were anesthetized with sodium pentobarbital, the diameter of each penis was measured and photographed, the skin of each penis was cut open, and the material (ADM or PVA) was implanted between the deep and superficial fascia. The penises were then sutured and photographed. Their penile lengths were measured and photographed at 1 week, 1 month, 2 months, and 3 months. The material was collected at 3 months. This study was approved by the Experimental Animal Ethics Committee of Guangzhou Seyotin Biotechnology Co. (study approval code: SYT2024029).

4.10. Morphological observation and case analysis

According to the experimental endpoints, the animals were humanely euthanized according to the guidelines of the Animal Welfare Act 3 months postoperatively. The implanted materials were surgically removed for imaging, and the hearts, livers, spleens, lungs, kidneys, penises, and testes were removed, fixed in formalin, embedded in paraffin, and stained with hematoxylin & eosin and Masson's trichrome.

4.11. Statistical analyses

All the experiments were repeated at least three times. The data are presented as the means ± standard deviations (n ≥ 3) and were analyzed via Excel. Excel was used to analyze the statistical data. The means ± standard deviations (n ≥ 3) were computed.

Ethics approval and consent to participate

This study was approved by the Experimental Animal Ethics Committee of Guangzhou Seyotin Biotechnology Co. (study approval code: SYT2024029).

CRediT authorship contribution statement

Rui Zheng: Writing – review & editing, Writing – original draft, Project administration, Formal analysis. **Wenwen Zhong:** Validation, Formal analysis. **Muyuan Chai:** Writing – review & editing, Methodology, Formal analysis, Conceptualization. **Xuetao Shi:** Supervision, Funding acquisition.

Declaration of competing interest

The authors declare that they have no known competing financial interests or personal relationships that could have appeared to influence the work reported in this paper.

Acknowledgments

R. Zheng and *W. Zhong* contributed equally to this work. The authors appreciate the financial support from the National Key Research and Development Program of China (2021YFB3800800), the National Natural Science Foundation of China (U22A20157, 32401141), the Guangdong Basic and Applied Basic Research Foundation (2022B1515130010, 2023A1515110794, 2024B1515040030), the Postdoctoral Fellowship Program of CPSF under Grant Number GZC20231080, and the China Postdoctoral Science Foundation (2024M751311).

Appendix A. Supplementary data

Supplementary data to this article can be found online at https://doi.org/10.1016/j.bioactmat.2024.08.039.

References

[1] D.Y. Yang, H.C. Jeong, K. Ko, S.H. Lee, Y.G. Lee, W.K. Lee, Comparison of clinical outcomes between hyaluronic and polylactic acid filler injections for penile augmentation in men reporting a small penis: a multicenter, patient-blinded/evaluator-blinded, noninferiority, randomized comparative trial with 18 months of follow-up, J. Clin. Med. 9 (2020), https://doi.org/10.3390/jcm9041024.

[2] C. Bettocchi, A.A. Checchia, U.G. Falagario, A. Ricapito, G.M. Busetto, L. Cormio, G. Carrieri, Male esthetic genital surgery: recommendations and gaps to be filled, Int. J. Impot. Res. 34 (2022) 392–403, https://doi.org/10.1038/s41443-022-00556-6.

[3] J. Lei, Y. Guo, C. Luo, X. Su, Preliminary application of a novel autologous scrotal dartos flap method for enlargement of penile girth in men with small penis syndrome, Plast. Reconstr. Surg. 150 (2022). https://journals.lww.com/plasreconsurg/fulltext/2022/11000/preliminary_application_of_a_novel_autologous.16.aspx.

[4] C. Zaccaro, D. Subirà, I. López-Diez, C. Manfredi, J.P. Ascensios-Vargas, I. Moncada-Iribarren, History and future perspectives of male aesthetic genital surgery, Int. J. Impot. Res. 34 (2022) 327–331, https://doi.org/10.1038/s41443-022-00580-6.

[5] M.H. Xing, S.W. Hou, O.A. Raheem, Aesthetic penile augmentation procedures: a comprehensive and current perspective, Curr. Urol. Rep. 23 (2022) 355–361, https://doi.org/10.1007/s11934-022-01123-8.

[6] H. Zhang, C. Jin, P. Zhang, Y. Wu, M. Zhang, W. Bai, Q. Li, T. Xu, X. Zhang, Human acellular dermal matrix augmentation phalloplasty surgery, Plastic Surgery 28 (2020) 161–166, https://doi.org/10.1177/2292550320928556.

[7] K.S. Vyas, A. Abu-Ghname, J. Banuelos, S.D. Morrison, O. Manrique, Aesthetic augmentation phalloplasty: a systematic review of techniques and outcomes, Plast. Reconstr. Surg. 146 (2020). https://journals.lww.com/plasreconsurg/fulltext/2020/11000/aesthetic_augmentation_phalloplasty__a_systematic.11.aspx.

[8] S.T. Ahn, J.S. Shim, W.J. Bae, S.W. Kim, J.J. Kim, D.G. Moon, Efficacy and safety of penile girth enhancement using hyaluronic acid filler and the clinical impact on ejaculation: a multicenter, patient/evaluator-blinded, randomized active-controlled trial, World Journal of Men's Health 39 (2021), https://doi.org/10.5534/WJMH.210007.

[9] M.R. Nowroozi, E. Amini, M. Ayati, H. Jamshidian, K. Radkhah, S. Amini, Applying extender devices in patients with penile dysmorphophobia: assessment of tolerability, efficacy, and impact on erectile function, J. Sex. Med. 12 (2015) 1242–1247, https://doi.org/10.1111/jsm.12870.

[10] G. An, F. Guo, X. Liu, Z. Wang, Y. Zhu, Y. Fan, C. Xuan, Y. Li, H. Wu, X. Shi, C. Mao, Functional reconstruction of injured corpus cavernosa using 3D-printed hydrogel scaffolds seeded with HIF-1α-expressing stem cells, Nat. Commun. 11 (2020) 2687, https://doi.org/10.1038/s41467-020-16192-x.

[11] Y. Liu, C. He, T. Qiao, G. Liu, X. Li, Q. Wan, Z. Zhu, Y. He, Coral-inspired hollow microneedle patch with smart sensor therapy for wound infection, Adv Funct Mater n/a (2024) 2314071, https://doi.org/10.1002/adfm.202314071.

[12] L. Casavantes, G. Lemperle, P. Morales, Penile girth enhancement with polymethylmethacrylate-based soft tissue fillers, J. Sex. Med. 13 (2016) 1414–1422, https://doi.org/10.1016/j.jsxm.2016.06.008.

[13] X. Zhang, Q. Sun, X. Liang, P. Gu, Z. Hu, X. Yang, M. Liu, Z. Sun, J. Huang, G. Wu, G. Zu, Stretchable and negative-Poisson-ratio porous metamaterials, Nat. Commun. 15 (2024) 392, https://doi.org/10.1038/s41467-024-44707-3.

[14] P. Chansoria, J. Blackwell, E.L. Etter, E.E. Bonacquisti, N. Jasiewicz, T. Neal, S. A. Kamal, J. Hoque, S. Varghese, T. Egan, J. Nguyen, Rationally designed anisotropic and auxetic hydrogel patches for adaptation to dynamic organs, Adv. Funct. Mater. 32 (2022), https://doi.org/10.1002/adfm.202207590.

[15] Y. Jiang, K. Shi, L. Zhou, M. He, C. Zhu, J. Wang, J. Li, Y. Li, L. Liu, D. Sun, G. Feng, Y. Yi, L. Zhang, 3D-printed auxetic-structured intervertebral disc implant for potential treatment of lumbar herniated disc, Bioact. Mater. 20 (2023) 528–538, https://doi.org/10.1016/j.bioactmat.2022.06.002.

[16] J.J. Elist, R. Valenzuela, J. Hillelsohn, T. Feng, A. Hosseini, A single-surgeon retrospective and preliminary evaluation of the safety and effectiveness of the Penuma silicone sleeve implant for elective cosmetic correction of the flaccid penis, J. Sex. Med. 15 (2018) 1216–1223, https://doi.org/10.1016/j.jsxm.2018.07.006.

[17] S.K. Wilson, A.-L.L. Picazo, Update on the Penuma® an FDA-cleared penile implant for aesthetic enhancement of the flaccid penis, Int. J. Impot. Res. 34 (2022) 369–374, https://doi.org/10.1038/s41443-021-00510-y.

[18] N. Schifano, P. Capogrosso, G. Antonini, S. Baldini, F. Scroppo, A. Salonia, N. Zerbinati, F. Dehò, The application of hyaluronic acid injections in functional and aesthetic andrology: a narrative review, Gels 9 (2023) 118, https://doi.org/10.3390/gels9020118.

[19] S.T. Ahn, J.S. Shim, W.J. Bae, S.W. Kim, J.J. Kim, D.G. Moon, Efficacy and safety of penile girth enhancement using hyaluronic acid filler and the clinical impact on ejaculation: a multicenter, patient/evaluator-blinded, randomized active-controlled trial, World Journal of Men's Health 39 (2021), https://doi.org/10.5534/WJMH.210007.

[20] M.I. Boiko, M.S. Notsek, O.M. Boiko, The efficacy of injection penile girth enhancement as an option for small penis syndrome management, Aesthet Surg J 44 (2024) 84–91, https://doi.org/10.1093/asj/sjad152.

[21] F. Rahimi, N. Ahmadkhani, A. Goodarzi, F. Noori, S. Hassanzadeh, S. Saghati, M. Khanmohammadi, A. Goodarzi, Gelatin-based hydrogel functionalized with taurine moieties for *in vivo* skin tissue regeneration, Biodes Manuf 6 (2023) 284–297, https://doi.org/10.1007/s42242-022-00227-x.

[22] T. Xu, G. Zhang, W. Bai, Q. Li, A. Yang, Q. Lin, T. Xu, X. Zhang, Complications and management of penile girth enhancement with acellular dermal matrix, J. Sex. Med. 16 (2019) 2011–2017, https://doi.org/10.1016/j.jsxm.2019.09.010.

[23] D.E. Panfilov, Augmentative phalloplasty, Aesthetic Plast. Surg. 30 (2006) 183–197, https://doi.org/10.1007/s00266-004-0153-y.

[24] M.G. Valverde, L.S. Mille, K.P. Figler, E. Cervantes, V.Y. Li, J. V Bonventre, R. Masereeuw, Y.S. Zhang, Biomimetic models of the glomerulus, Nat. Rev. Nephrol. 18 (2022) 241–257, https://doi.org/10.1038/s41581-021-00528-x.

[25] X. Liu, H. Wang, J. She, Q. Zhang, Q. Hu, D. Li, H. Wu, X. Ye, R. Diao, X. Shi, L. Wang, An anti-fibroblast adhesion and anti-inflammatory hydrogel film combined with VEGF for intrauterine adhesion prevention, Chem. Eng. J. 466 (2023), https://doi.org/10.1016/j.cej.2023.143144.

[26] Y. Huang, X. Zhao, C. Wang, J. Chen, Y. Liang, Z. Li, Y. Han, B. Guo, High-strength antibacterial composite cryogel for lethal noncompressible hemorrhage hemostasis: synergistic physical hemostasis and chemical hemostasis, Chem. Eng. J. 427 (2022) 131977, https://doi.org/10.1016/j.cej.2021.131977.

[27] S. Jung, B. Pant, M. Climans, G. Curtis Shaw, E.-J. Lee, N. Kim, M. Park, Transformation of electrospun Keratin/PVA nanofiber membranes into multilayered 3D Scaffolds: physiochemical studies and corneal implant applications, Int J Pharm 610 (2021) 121228, https://doi.org/10.1016/j.ijpharm.2021.121228.

[28] J. Yang, Z. Chen, C. Gao, J. Liu, K. Liu, X. Wang, X. Pan, G. Wang, H. Sang, H. Pan, W. Liu, C. Ruan, A mechanical-assisted postbioprinting strategy for challenging bone defects repair, Nat. Commun. 15 (2024) 3565, https://doi.org/10.1038/s41467-024-48023-8.

[29] C.-F. He, Y. Sun, N. Liu, K. Yu, Y. Qian, Y. He, Formation theory and printability of photocurable hydrogel for 3D bioprinting, Adv. Funct. Mater. 33 (2023) 2301209, https://doi.org/10.1002/adfm.202301209.

[30] D. Liu, Y. Cao, P. Jiang, Y. Wang, Y. Lu, Z. Ji, X. Wang, W. Liu, Tough, transparent, and slippery PVA hydrogel led by syneresis, Small 19 (2023), https://doi.org/10.1002/smll.202206819.

[31] M. Chai, Z. Zhai, X. Liu, K. Wu, Y. He, S. Ostrovidov, H. Wu, L. Bian, X. Shi, Bionic artificial penile Tunica albuginea, Matter 6 (2023) 626–641, https://doi.org/10.1016/j.matt.2022.11.032.
[32] S. Wang, Z. Wang, W. Yang, Z. Xu, H. Dai, F. He, S. Yan, X. Shi, *In situ*-sprayed bioinspired adhesive conductive hydrogels for cavernous nerve repair, Adv. Mater. 36 (2024), https://doi.org/10.1002/adma.202311264.
[33] W. Yang, W. Zhong, S. Yan, S. Wang, C. Xuan, K. Zheng, J. Qiu, X. Shi, Mechanical stimulation of anti-inflammatory and antioxidant hydrogels for rapid Re-epithelialization, Adv. Mater. 36 (2024), https://doi.org/10.1002/adma.202312740.
[34] S.R. Stauffer, N.A. Peppast, Poly(vinyl alcohol) hydrogels prepared by freezing-thawing cyclic processing, Polymer (Guildf) 33 (1992) 3932–3936, https://doi.org/10.1016/0032-3861(92)90385-A.
[35] S. Lin, X. Liu, J. Liu, H. Yuk, H.-C. Loh, G.A. Parada, C. Settens, J. Song, A. Masic, G.H. McKinley, X. Zhao, Anti-fatigue-fracture hydrogels, Sci. Adv. 5 (2024) eaau8528, https://doi.org/10.1126/sciadv.aau8528.
[36] A. Berardo, M.V. Mascolini, C.G. Fontanella, M. Contran, M. Todesco, A. Porzionato, V. Macchi, R. De Caro, R. Boscolo-Berto, E.L. Carniel, Mechanical characterization of the male lower urinary tract: comparison among soft tissues from the same human case study, Appl. Sci. 14 (2024) 1357, https://doi.org/10.3390/app14041357.
[37] D. Veale, S. Miles, S. Bramley, G. Muir, J. Hodsoll, Am I normal? A systematic review and construction of nomograms for flaccid and erect penis length and circumference in up to 15 521 men, BJU Int. 115 (2015) 978–986, https://doi.org/10.1111/bju.13010.
[38] R. Ponchietti, N. Mondaini, M. Bonafè, F. Di Loro, S. Biscioni, L. Masieri, Penile length and circumference: a study on 3,300 Young Italian males, Eur. Urol. 39 (2001) 183–186, https://doi.org/10.1159/000052434.
[39] Z. Awwad, M. Abu-Hijleh, S. Basri, N. Shegam, M. Murshidi, K. Ajlouni, Penile measurements in normal adult Jordanians and in patients with erectile dysfunction, Int. J. Impot. Res. 17 (2005) 191–195, https://doi.org/10.1038/sj.ijir.3901272.
[40] G. He, Y. Xian, H. Lin, C. Yu, L. Chen, Z. Chen, Y. Hong, C. Zhang, D. Wu, An injectable and coagulation-independent Tetra-PEG hydrogel bioadhesive for postextraction hemostasis and alveolar bone regeneration, Bioact. Mater. 37 (2024) 106–118, https://doi.org/10.1016/j.bioactmat.2024.03.015.
[41] Z. Zhu, H. Ye, K. Zhang, G. He, Z. Pan, Y. Xian, Y. Yang, C. Zhang, D. Wu, Naturally, derived injectable dual-cross-linked adhesive hydrogel for acute hemorrhage control and wound healing, Biomacromolecules 25 (2024) 2574–2586, https://doi.org/10.1021/acs.biomac.4c00105.